AMMap Tool for Additive Manufacturing Design, Alloy Discovery, and Path Planning

Alexander M. Richter [a], Adam M. Krajewski[a], Zhening Yang [a], Allison M. Beese [a], Zi-Kui Liu[a]

a. Department of Materials Science and Engineering, The Pennsylvania State University, PA, USA

Corresponding Author: A. M. Richter | University Park, PA | amr8004@psu.edu

March 20, 2025

Abstract

Compositionally complex materials (CCMs), such as functionally graded materials (FGMs) made by additive manufacturing (AM) often form undesired phases or cracks, negatively affecting the build. Equilibrium thermodynamic calculations and solidification simulations, such as Scheil-Gulliver, can be used to predict feasible compositions or compositional paths, acting as constraints before empirical or machine learning models are applied to predict properties of interest. In addition, additional analysis of solidification simulations can be used to predict hot-cracking using various criteria to further account for manufacturability. To define and navigate the high order chemical systems of CCMs/FGMs, the open-source tool, AMMap, has been developed utilizing open models and CALPHAD methods for thermodynamic computation. AMMap explores spaces constructed with the nimplex library, using a novel algorithm to represent high-dimensional systems as graphs that can be joined into homogeneous structures and explored with graph traversal algorithms to automate the path-design process. This method allows the use of existing high-performance gradient descent, graph traversal search, and other path optimization algorithms to automate the path-design process with as little prior bias as possible.

Contents

1 Introduction

1.1 Background

Additive manufacturing (AM) methods enable the creation of complex geometries and the integration of multiple materials within a single build, and are widely used in many industries, including aerospace, automotive, consumer products, and biomedical [1]. The ability to incorporate nanomaterials and composite materials into AM processes has opened new avenues to improve the mechanical, thermal, and electrical properties of manufactured parts [2]. The high level of control in AM is particularly beneficial for producing functionally graded materials (FGMs), which can mitigate the deleterious effects of abrupt interfaces between dissimilar materials that cannot be directly joined. FGMs are multi-material components with composition, mesostructures, and/or microstructures that vary with position through a build that can afford FGMs multi-functionality [3] or enable dissimilar metals to join smoothly [4]. In joining dissimilar materials, FGMs can be used to avoid the formation of brittle topologically close-packed (TCP) phases, known to cause component failure [5] as well as to mitigate other difficulties, such as differences in thermal expansion coefficients and chemical incompatibilities, which can lead to residual stresses and weakened interfaces. By leveraging advanced AM techniques, these challenges can be mitigated, enabling the production of high-performance, multi-material components with tailored properties for

specific applications. To create FGMs that successfully transition between different materials, non-linear composition paths, intermediate materials, or composition gradients can be employed. These methods help avoid issues such as TCP phases and dissimilar property gradients, which may lead to stress-induced cracking [6]. To avoid expensive trial-and-error methods, computational design techniques can predict material behavior, such as phase formation more efficiently. For example, a path designed to avoid TCP phases between two critical, dissimilar metal alloys—from stainless steel to Ti-6Al-4V FGM—was successfully created by incorporating V, Cr, and NiCr as intermediaries [5]. Leveraging these computational techniques allows for the design of materials with optimized properties and enhanced performance, ensuring the reliability and functionality of the final components.

One such computational technique is the CALculation of PHAse Diagrams (CALPHAD) method for the calculation of phase formation of alloys under both equilibrium and rapid-solidification conditions. With knowledge of processing parameters and CALPHAD calculations, a build-path that avoids failure can be predicted, enabling the design of an FGM efficiently and effectively. However, applying models such as the CALPHAD method to the chemistry of these materials can be complex because of the difficulty in representing alloy compositions and their changes in high-dimensional space. Since the means of calculation are available, the primary goal then becomes efficiently performing calculations and finding a design path to build that meets any other criteria such as property minimizations. The high-dimensional phase space required to model complex alloy systems can be computationally intensive and challenging to navigate. Despite these challenges, the CALPHAD method enables precise thermodynamic modeling, allowing for the optimization of alloy compositions and the prediction of phase behaviors under various conditions and is invaluable to the design process. By addressing these complexities, it is possible to improve the methods to design FGMs with tailored properties, enhancing their performance and reliability in various applications.

1.2 Contemporary Challenges and Needs in Compositionally Complex Materials Design

A number of recent works have been produced to computationally design FGMs, highlighting the community interest in modeling them [7]–[13]. Kirk *et al.* [7], [8] used a constraint satisfaction algorithm for robotic motion planning based on equilibrium thermodynamic calculations from the CALPHAD approach. In the process of joining materials, non-equilibrium heating and cooling can result in solute segregation within the liquid phase during solidification, which can be difficult to predict through equilibrium thermodynamic calculations alone. Research by Bocklund *et al.* [9], [10] demonstrated that Scheil-Gulliver simulations provide more accurate predictions of phase formation in a Ti-Invar FGM compared to pure equilibrium calculations. Scheil-Gulliver simulations are employed to forecast phase formation under rapid cooling conditions. These simulations operate under specific assumptions: no diffusion occurs in the solid phase, equilibrium exists at the solid-liquid interface, and infinite diffusion takes place in the liquid phase. Moustafa *et al.* [11] proposed a Scheil-Gulliver ternary projection diagram for the Fe-Cr-Al system using Thermo-Calc, revealing significant differences in phase formation compared to equilibrium predictions. Sun *et al.* [13] used a CALPHAD-based tool `MaterialsMap` implementing both Scheil-Gulliver and equilibrium thermodynamic calculations and demonstrated by joining dissimilar pure Al to Cu with an Ag interlayer. Beyond phase formation predictions, Yang et al. [12] successfully applied Scheil-Gulliver simulations to forecast hot cracking in FGMs. Their study predicted hot cracking in 316L Stainless Steel (SS316) to Ni-20Cr, to Cr, to V, and finally Ti-6Al-4V using various hot cracking criteria from the welding and joining literature.

The development of an open-source Python tool for multi-property and multi-constraint design of compositionally varying materials, including high-throughput CALPHAD calculations, presents an opportunity to address key limitations in the existing approaches dominated by manual path planning based on precomputed maps. Furthermore, while current methods often typically operate in isolation with rigid coding structures, a more flexible and extensible framework enables more consistent incremental improvements and additions to fit new niche applications by emphasizing a modular architecture that allows for easy integration of new calculations through standalone customizable templates. Such templates can resemble typical single-purpose code modules attached to scientific publications, written in Python or other language with foreign function interface (FFI), enabling calculation of objectives or constraints of interest after a set of constants is populated.

To effectively design and optimize materials using automation, it is essential to define a comprehensive set of information and constraints. This includes specifying the types of calculations to be performed, the relevant property criteria, and the design spaces in which models will operate. The following YAML examples illustrate how to structure this information for a FGM design.

The initial step in multi-property and multi-constraint

design involves meticulously defining the necessary information and constraints. This foundational phase includes specifying the types of calculations to be performed, such as equilibrium and Scheil-Gulliver solidification, and identifying the relevant property criteria to be considered. For instance, in a given example, constraints might include maintaining specific equilibrium phases at a set temperature and pressure, ensuring certain phases are present or absent, and adhering to limits on properties like density and cracking susceptibility. By clearly outlining these constraints and optimization criteria, designers can effectively navigate complex phase diagrams and achieve the desired material properties, ensuring a robust and efficient design process.

```yaml
name: "StainlessSteel316L_to_Ti64"
description: "Path planning across several ternary
↪  phase diagrams from Stainless Steel (Ni9.6 Cr19.9
↪  Fe70.5) to Ti-6Al-4V (Ti0.862 Al0.102 V0.036)"
nDivisionsPerDimension: 12
constraints:
  - type: equilibrium phases
    temperature: 900
    pressure: 1
    feasiblePhases:
     - FCC_A1
     - BCC_A2
     - HCP_A3
    requiredPhases:
     - BCC_A2
    infeasiblePhases:
     - LIQUID
     - SIGMA
  - type: scheil-gulliver solidification
    startTemperature: 2500
    feasiblePhases:
     - FCC_A1
     - BCC_A2
     - HCP_A3
  - type: LC density
    max: 11.5
  - type: AM cracking susceptibility
    criteria:
     - Kou
     - iCSC
     - sRDG
```

It is crucial to define the spaces in which both thermodynamic and machine learning (ML) models operate, as well as the spaces available for exploring potential solutions. For instance, design spaces such as stainless steel (SS) to V and Ti-6Al-4V to Cr are defined by their constituent elements and associated thermodynamic databases, which must be capable of representing the desired space. These spaces provide the foundational data required for accurate modeling and simulation. Within these elemental spaces, specific design spaces like SS, Ni-Cr-V, and Ti-6Cr-4V are delineated based on their component compositions and interconnected through common representable spaces, such as Ni-Cr in SS and Ni-Cr-V and Cr-V with Ti-6Al-4V. These design spaces serve as the operational domains for the models, enabling the exploration of various phase equilibria, solidification paths, and property optimizations. By clearly defining these spaces, designers can leverage both thermodynamic and ML models to navigate complex material systems and identify optimal solutions that meet the specified constraints and criteria.

```yaml
elementalSpaces:
  - name: SS_V
    elements:
      - Ni
      - Cr
      - Fe
      - V
    tdb: Bobbio2021.tdb
  - name: Ti64_Cr
    elements:
      - Ti
      - Al
      - V
      - Cr
    tdb: MyTitaniumAlloysDatabase.tdb

designSpaces:
  - name: SS
    elementalSpace: SS_V
    components:
      - [0.096,0.200, 0.704, 0]  # SS
      - [0, 1, 0, 0]             # Cr
      - [1, 0, 0, 0]             # Ni
    stitch:
     - edge: Cr-Ni
       targetDesignSpace: Ni_Cr_V # Must have Cr-Ni
  - name: Ni_Cr_V
    elementalSpace: SS_V
    components:
      - [1, 0, 0, 0]             # Ni
      - [0, 1, 0, 0]             # Cr
      - [0, 0, 0, 1]             # V
    stitch:
      - edge: Cr-V
        targetDesignSpace: Ti64_Cr_V
  - name: Ti64_Cr_V
    elementalSpace: Ti64_Cr
    components:
      - [0.862, 0.102, 0.036, 0] # Ti64
      - [0, 0, 1, 0]             # V
      - [0, 0, 0, 1]             # Cr
```

The final component in this improved design process involves defining the specific goals associated with the problem. These goals can vary depending on the context, such as path calculation in the design of FGMs or the search for maximum property values in the context of singular material design, like High Entropy Alloys

(HEAs). For instance, the path plan outlined in the YAML file specifies a transition from the SS design space at a particular position to the Ti-6Cr-4V design space. This path calculation is essential for FGMs, where a gradual transition between materials with different properties is desired. In contrast, for HEAs, the focus might be on identifying compositions that maximize certain properties, such as strength or corrosion resistance. By clearly defining these goals, designers can effectively utilize the defined design spaces and constraints to achieve the desired outcomes, whether it be a smooth gradient in FGMs or optimal properties in HEAs.

```yaml
pathPlan:
  - designSpace: SS
    position: [12, 0, 0]
  - designSpace: Ti64_Cr_V
    index: -1
```

This approach highlights the potential of utilizing both machine and human-readable formats to streamline an automated workflow with reusable problem statements. Known information, such as feasible and infeasible phases, can be presented as constraints for simulation, along with desired property results like density. The design space can be defined not only by pure elemental boundaries but also by specific alloys within a database, such as Stainless Steel. Desired paths can be mapped from starting points, considering constraints to identify optimal routes. This structured input can then be used to generate custom Python scripts for specific purposes, or callables, based on pre-generated templates. Utilizing templates ensures uniformity and repeatability across new systems. When new properties need to be implemented, the generation scripts and templates can be modified to accommodate different model properties, maintaining consistency and adaptability in the workflow. By implementing a system of reusable problem statements, data structures, and custom callables, researchers can efficiently create solution spaces, calculate properties, and plan optimal manufacturing paths. The tool's design prioritizes metadata retention, ensuring that the provenance and context of calculations are preserved, which is crucial for reproducibility and future analysis. Furthermore, its adaptability makes it an ideal platform for incorporating ML models as "oracle" callables, enabling the seamless integration of AI-driven predictions into the design process. Perhaps most importantly, this framework facilitates the rapid packaging and distribution of customized tools alongside publications, enhancing the reproducibility and dissemination of research findings. This approach not only streamlines the current workflow but also paves the way for more collaborative and iterative advancements in AM material design.

Additionally, designing materials for AM presents several challenges that cannot be easily overcome by brute force ML approaches alone. The space between well-studied alloys remains largely unexplored, making extrapolation difficult and risky. The vast design space requires highly efficient search strategies to be practical. This compositional space of alloys is often represented as a simplex rather than Cartesian coordinates, necessitating specialized optimization techniques. Currently, tools for AM material design are fragmented, each addressing only a specific aspect of these problems. To address these issues coherently, there is a pressing need for a unified, extensible framework that integrates various tools and methodologies. Such a framework would enable end-users to efficiently explore the design space, easily adjust parameters, and reproduce results. This approach would not only streamline the material design process for AM but would also facilitate the development of novel materials with tailored properties for specific applications.

To reach this end , `AMMap`, a python tool for **A**dditive **M**anufacturing **Map**ping of Compositional Spaces with Thermodynamic, Analytical, and Artificial Intelligence Models is developed. Its purpose is to enable design of additively manufactured materials, particularly FGMs, by enabling easy description of the complex space made available and necessary for this purpose. It helps guide compositional design through the currently implemented methods and by providing a framework for allowing any number of different criteria for design. Currently, high-throughput equilibrium and Scheil-Gulliver simulation can be used for phase formation information as well as different criteria for the crack susceptibility of a given alloy to efficiently plan a material. Some chemical information that can be found via linear combination such as density or provided from existing python tools such as root mean square atomic displacement are also included. By virtue of being open-source and python based, it allows easy tailoring of new critera from already available python tools and data or creation of new tools. Ultimately, `AMMap` is made for putting machine learning, CALPHAD, established literature models, graph theory, and path planning into a unified reproducible framework.

While originally designed as an AM tool, `AMMap` is rather a complex material design space tool, making it highly applicable to HEA design as well. HEAs contain multiple principal elements [14], in contrast to conventional alloys that typically have one principal element, and emerged in 2004 through the work of Yeh *et al.* [15] and

Cantor *et al.* [16]. The inclusion of multiple principal elements can lead to materials with interesting properties, such as high strength, corrosion resistance, and radiation resistance. However, the multiple principal elements also lead to a high-dimensional space needed to represent them, where `AMMap` proves beneficial.

Many types of high entropy materials exist, and `AMMap` is designed to be able to adapt to any type. Multi-Principal Element Alloys (MPEAs) or HEAs [15]–[19] are the most directly related, as the existing CALPHAD metal databases allow for the full application of the implemented tool, alongside the ability to apply more HEA-specific tools to the design space. High Entropy Ceramics (HECs) [20], High Entropy Metallic Glasses (HEMGs) [21], and organic High Entropy Polymers (HEPs) [22]–[24] would also benefit from `AMMap`. The ability to automatically create and represent the compositions in a computer-readable space allows for the application of ML and other computational tools to explore and design such materials.

HEAs excellent mechanical properties, including hardness [25], ductility [26], room temperature strength [27], and refractory strength [28]–[30], and functional properties, such as superconductivity [31]–[33], catalytic performance [34], [35], and magnetic behavior [36]–[38]. Physical, mathematical, and ML models for property prediction on HEAs would greatly benefit from `AMMap`'s simplex space, creating uniform spaces where property gradients can be mapped and used in HEA design or exploration.

2 Methods and tools

2.1 Representing Compositional Space as Traversable Graph with `nimplex`

In its core, `AMMap` leverages the recently-published algorithm for construction of graphs representing all discretized compositions (e.g., at 1 or 5%) in a given system and all possible equidistant transitions between neighbors [39] implemented through `nimplex` (NIM library for simPLEX spaces). Such graphs enable efficient representations of non-Euclidean compositional design spaces, which underlay majority of materials discovery efforts, while maintaining correctness of distances, simplified thanks to the equidistant nature, and high performance of the statically-allocated data structure, even for complex high dimensional spaces. Furthermore, graphs are inherently suitable for joining into larger homogeneous representations, which can be leveraged to simultaneously explore many adjacent problems, as showcased later in Section 3.2.

Graphs can also be iteratively explored through numerous established algorithms (see Section 2.2) to traverse the space in some informed fashion or establish continuous paths between feasible points, such as one depicted in the Figure 1 example, to facilitate design of FGMs.

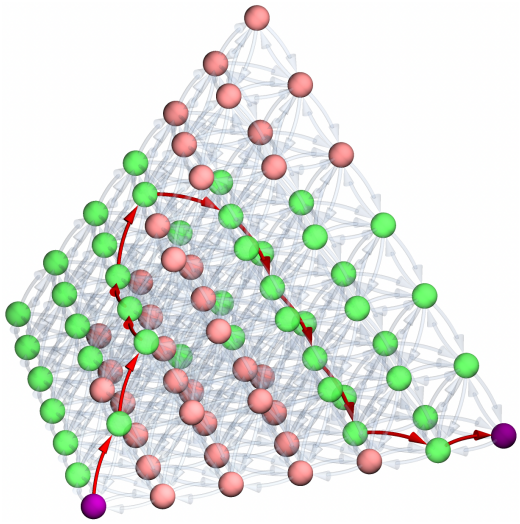

Figure 1: A quaternary compositional graph with 6 divisions per dimension resulting in 84 nodes (discrete compositions) and 672 edges (possible moves). A set of nodes has been manually selected (highlighted in pink) to depict a toy example of infeasible points, which forces a non-trivial path (highlighted in red) to traverse between start and end nodes (purple).

`nimplex` has been written in Nim language [40] enabling high-performance computation and data storage, but can also be used to (1) produce NumPy [41] array files from command line interface (CLI) and (2) be compiled with a Python interface covering all main use cases, both of which can be leveraged by `AMMap`. Furthermore, in addition to graph construction, `nimplex` can be used by advanced `AMMap` users to extend its functionality through simplex space samplings, uniform grids, and other methods it provides.

2.2 Path Planning

Graph traversal and path planning are well explored fields of mathematics and computer science, with many high-performance libraries implementing algorithms that can carry guarantees of optimality if certain characteristics are met by the explored graph. For instance, the A* algorithm [42] can be used over compositional graphs computed by `nimplex` to find *the* shortest feasible compositional path while exploring the mathematically guaranteed least number of nodes [43], i.e., performing least calculations or ML model calls.

For demonstration purposes, `AMMap` tutorials use the Dijkstra algorithm, implemented in the pure python

pathfinding package, which is a widely-used algorithm for finding the shortest path while meeting the basic design specifications of the tool. At the same time, nimplex/AMMap's straightforward graph representation can be quickly adapted to most of the popular frameworks or explored with custom scripts in any language of choice.

2.3 Equilibrium and Scheil-Gulliver simulations

The CALPHAD method is used to calculate phase formation in alloys by minimizing the Gibbs energy of a system with many individual phases, expressed as functions of temperature, pressure, and composition [44], [45]. This method considers both stable and unstable regions, allowing for precise thermodynamic modeling and optimization of alloy compositions [46]–[48]. To predict phase formation, two different types of simulations are performed. For slow cooling rates, equilibrium thermodynamic calculations can be used to predict phases formed, while fast cooling rates can be predicted using Scheil-Gulliver simulations [49], [50].

Equilibrium thermodynamic calculations involve using thermodynamic models to predict phase stability and formation in alloy systems by minimizing Gibbs energy. These calculations are performed using the open-source tool pycalphad [51], which returns phase formed and their amounts for a given composition under constant temperature, pressure, and composition. Equilibrium calculations are applicable for slow cooling rates, providing information on phases that may be present in the system. Despite true equilibrium rarely being achieved during AM manufacturing, these calculations are invaluable for predicting the equilibrium state and understanding solid-state transformations that could occur. Equilibrium is also useful in AM due the repeated thermal cycles and post-processing heat-treatments which can lead to states closer to true equilibrium.

To more completely capture the phase formation during AM, Scheil-Gulliver simulations are performed. Scheil-Gulliver simulations operate with three main assumptions: local equilibrium at the solid/liquid interface, perfect mixing in the liquid phase due to rapid diffusion, and no diffusion in the solid phase. These simulations predict the formation of solid phases that might not appear in equilibrium simulations because of the changes in composition of the liquid phase. This is relevant to fast cooling processes like AM or welding, where diffusion in the liquid and Marangoni flow (liquid transfer on the interface of the solid and liquid as a result of surface tension) cause mixing to occur in the liquid. Scheil-Gulliver simulations have successfully been used to study phase formation in AM FGMs by Bocklund et al. [9], [10] where Ni_3Ti was shown experimentally to form in a Ti-6Al-4 V and Invar FGM, which matched with Scheil-Gulliver but not equilibrium simulation. AMMap performs Scheil-Gulliver simulations using a python package based on pycalphad called scheil [9] which returns fractions and compositions of solid and liquid phases at various temperatures under a given condition and efficiently delineates the phase boundaries formed during the rapid cooling process. The scheil package was further improved in the work by Hui et. al. to distinguish order/disorder of phases [13] allowing for consideration of order-disorder transition. Scheil and pycalphad can be used in a high-throughput process in order to better systematically work through the complex space described by the nimplex grid.

Hybrid Scheil-equilibrium method was developed to bridge the gap between equilibrium and Scheil simulations, to account for both solidification microsegregation and solid-state transformations. By first performing a Scheil simulation and then conducting equilibrium simulations along the solidification path, solid-state phase transformations below the solidus temperature can be predicted, while accounting for microsegregation during solidification. Although diffusion is ignored in the hybrid Scheil-equilibrium method, it has proven valuable for predicting solid-state phase transitions in FGMs during the reheating process in fabrication [12] and for predicting phases during the post heat treatment [52].

2.4 Including Cracking and Other Criteria

Successful creation of AM part relies on more than just phase formation. One of the values of AMMap is that it has been designed so that any property that can be joined to the composition can be easily implemented together in the space for consideration.

Primary demonstration of this ability is done using the hot-cracking susceptibility of a material. This is important because AM FGMs have been shown to crack, even when deleterious phases were zero or very low [5], [53]–[56] due to liquation cracking resulting from the remelting of interdendritic precipitates with low melting temperature, solidification cracking due to interdendritic stress and lack of liquid backfilling at the end of solidification process, or thermal stress accumulation from CTE mismatch during cooling.

Yang et. al. [12] showcased the ability to utilize five existing hot cracking criteria [[57], [58]] to determine the susceptibility of a composition to hot cracking and its value in predicting crack formation in mul-

tiple FGMs. These criteria quantify hot cracking susceptibility by evaluating the temperature drop within the cracking-susceptible range during solidification – specifically, when the solid fraction is sufficient to form solid networks, but liquid persists in the channels. A rapid temperature drop indicates an increased likelihood of forming continuous liquid films in the interdendritic region, higher shrinkage of the solid network, and the potential formation of interdendritic precipitates with low melting temperatures, all of which contribute to hot cracking. These criteria can be calculated using information gained from Scheil-Gulliver simulation and have been implemented into AMMap as examples of additional information that can be used for AM material design.

Additional property models are also available and can be easily implemented thanks to the modular nature of AMMap. Included in the release version of the package are (1) a density callable based on linear combination of atomic densities, (2) a root mean square atomic displacement (RMSAD) ML model for BCC HEAs created by Tandoc *et al.* [59], which can be used as a relative strength surrogate, and (3) an intrinsic ductility model for BCC HEAs by Hu *et al.* [60], which can be used to avoid brittle solid solution alloys.

3 Results

3.1 AMMap Structure

AMMap is a Python-based open-source software, hosted on Github, designed to simplify the process for material design while also enabling easy expansion of capabilities. The workflow, presented in Figure 2, is showcased from the starting point of the conceptualization of the problem to be solved (step 0), to the resulting (a) precise, machine-readible problem definition (blue), (b) problem solution and explored space data (purple), (c) readily reproducible and reusable problem-specific tool (yellow), which can be attached to publications based on AMMap as well-defined reusable supplemental information.

The core requirement of AMMap, when applied to exploration of materials through CALPHAD methods, are the thermodynamic databases (TDBs) covering the applicable compositional space or spaces. This requirement is essential because the TDB file contains the necessary thermodynamic data for the various elements and phases involved in the compositions being studied, which are used as direct constraints, sach as constraints for applicability of a model (e.g., [60] or [59] work only if only BCC phase is present), or to inform models taking phase information as input [61]). Thus, without applicable TDBs, no thermodynamic calculations can occur, limiting AMMap to only purely compositional models.

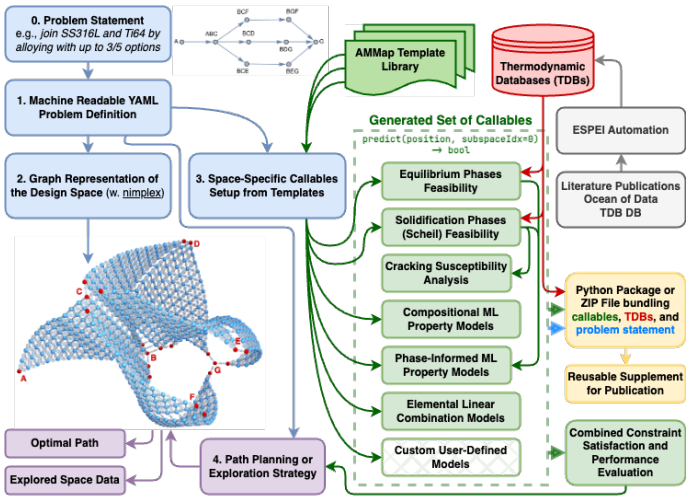

Figure 2: Flowlike structure of AMMAP from Problem Statement to Optimal Path

Multiple TDBs, commonly needed to model dissimilar materials, can be seamlessly integrated using nimplex's "stitching" functionality, by creating complex spaces unique to each TDB and then joining equivalent points, edges, faces, or more generally, any common subspaces between any number of systems. This integration results in a singular graph that any path-planning algorithm can navigate, while keeping track of a set of individualized callables to perform appropriate CALPHAD calculations and ML predictions. This process can be highly complex if done manually; thus, AMMap streamlines it through automated use of templates and scripts.

To perform aforementioned automations, AMMap uses a YAML input format to define the problem and generate the necessary scripts because YAML is both computer and human-readable similar to the example in section 1.2. The YAML file specifies the requested TDBs, or in the future specific model weights, for a singular composition space and the desired property calculations, creating all the necessary callables to perform the assessments and any additional analysis.

The process results in modular callables created for all composition and TDB combinations for equilibrium, Scheil, and any composition-dependent properties such as density. These callables enable the execution of CALPHAD calculations that require TDB specific information. The process is facilitated by easily modifiable callable builders, which use pre-made templates to fill in the necessary information from the YAML input. The space can then be created in a Jupyter notebook, edges stitched, and efficiently calculated over using parallel-processing Python modules. Additionally, the example notebooks showcase the necessary scripts to perform Infeasibility

Gliding technique, introduced by the authors in a separate paper, where the design space is iteratively explored by evaluating neighbors of feasible points, resulting in calculations being done only over the continuous feasible regions containing starting points and the infeasible surface bounding it. Such approach, skipping calculations of insides of infeasible regions and disconnected feasible regions (not contributing to path planning), significantly reduces computational cost of running AMMap, as shown later in 3.2, without affecting the final result.

One key benefit of this structure style is that all resulting callables and TDBs can be easily bundled together and attached to any work where AMMap was used to supplement repeatability of the study. Additionally, AMMap is designed to be easily extensible to adding new callables. This extensibility is achieved through its modular architecture, which allows developers to create new callables by defining additional templates and scripts. The use of YAML input files ensures that new properties and calculations can be specified without altering the core codebase. Furthermore, the integration with Jupyter notebooks and parallel-processing modules means that new functionalities can be tested and implemented efficiently, making AMMap a versatile tool for ongoing research and development in material design.

The end result of running AMMap is a simplex graph of nodes with associated property information such as phases present after solidification according to Scheil which can then be used with any existing path planning tool to design an optimal path for an FGM.

3.2 Demonstration joining SS316 to Ti-6V-4Al

As mentioned previously, joining stainless steel to titanium alloys is a desirable FGM due to their associated properties, but remains a complex problem due to obstacles including formation of known TCP phases such as the σ phase forcing non-linear paths involving other alloys selected from a spectrum of candidates. In particular, there is a significant interest in design of a path from stainless steel (SS) 316 to aerospace-grade titanium grade Ti-6Al-4V, which are idealized here as $Cr_{19}Fe_{72}Ni_9$ and $Ti_{90}V_{10}$ chemical compositions in Cr-Fe-Ni-Ti-V quinary space, to remain consistent with past design studies. Most critically Bobbio *et al.* [5] calculated feasibility, defined as less than 10 at% of TCP phases, for all ternary systems using Scheil and equilibrium calculations, manually fitting them together to form a path from SS316 in the Cr-Fe-Ni ternary, to $Ni_{80}Cr_{20}$, to pure Cr, to pure V, and finally to Ti-6Al-4V, and then experimentally validated the path through the fabrication of the FGM.

While it is not challenging to navigate the space to find *a* path, as feasible regions of intermediate alloys found in [5] create clear conductivities, it still can be used to showcases the possible complexity of FGM path planning if the goal is to find an optimal path per a defined objective such as *the* shortest continuous path.

Figure 3 showcases the high complexity of *how* the 10 possible ternaries in the Cr-Fe-Ni-Ti-V, a system with just 5 elements, can be combined together to consider all possible moves between them.

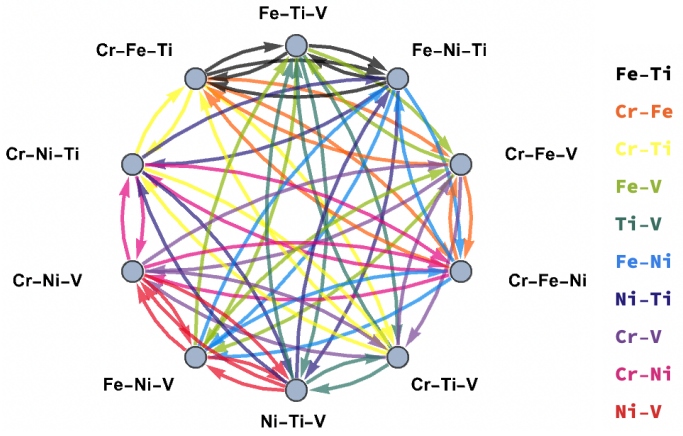

Figure 3: Schematic graph of the 10 ternary systems and 30 binary connections between them.

The same space has been selected to demonstrate the ability of AMMap to improve this process via automation and efficient space designation and exploration. The same TDBs were used to ensure that there were no differences in the computational results. A YAML file was created, linking the respective ternary spaces to their respective TDBs, and Scheil and equilibrium results were specified as desired. The AMMap script for automated callable construction was then used to generate them, followed by generation and stitching of the 10 ternary spaces, each containing 703 discrete compositions, done within a Jupyter notebook tutorial.

The equilibrium and Scheil results were run in parallel utilizing supercomputer resources. To avoid excessive computational time for the Scheil simulations, Infeasibility Gliding (IG) was used to reduce the total number of points calculated. For constraints, equilibrium was performed at 1000 K, and Scheil took 1K steps from 2500K until fully solidified. All ordered and disordered FCC, BCC, and HCP phases were considered feasible, with the presence of other phases making a composition infeasible. Results, feasibility, and the simplex stitching graphs were saved as JSON files. Using IG, 4439 out of 7030 points were avoided in equilibrium simulations, and 3729 infeasible points were avoided in Scheil simulations. The shortest path was then found from the position

on the grid most similar to the SS316 composition, represented as 18.8Cr-71.9Fe-9.4Ni to Ti-10V using Dijkstra's algorithm. The full result can be seen in Figure 4. Here, the difficulty in manual path finding becomes clear, as in order to visually represent that each ternary is connected to six other ternaries, an amorphous shape results.

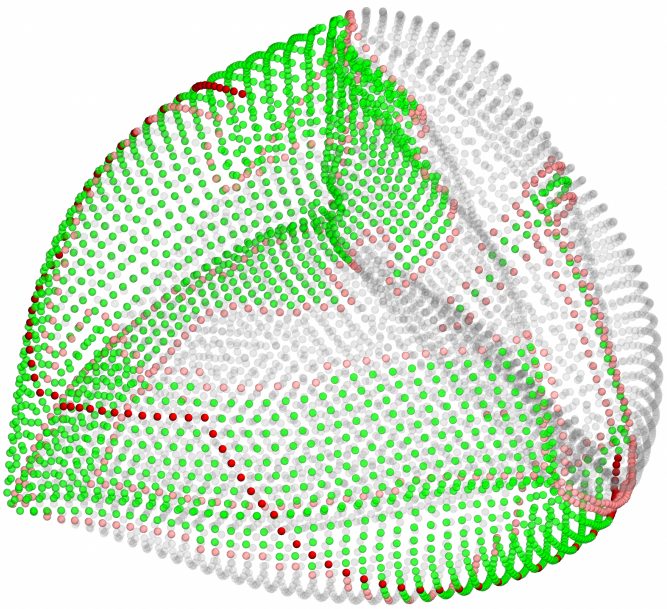

Figure 4: Lower-dimensional (3D) visualization of the graph representation of the search space with the identified path (crimson), feasible compositions (green), infeasible compositions (pink), and not-calculated interiors of the infeasible regions (gray).

The automated path found differed from the previously manually identified path, with the only constraint that it was the shortest possible route avoiding any possible formation of infeasible (e.g. TCP) phases. The resulting path can be seen in Figure 5, which shows 3 ternary systems selected from Figure 4 through which the path passed. The new path navigated closely around the infeasible region in the Cr-Fe-Ni ternary, to the Fe-Cr binary, into the Fe-Cr-V, to Cr-V, to Ti-V to Ti-10V. This differs mainly because the machine created path navigates around infeasible regions in a C-like shape in the Cr-Fe-Ni and Cr-Fe-V systems to ensure the shortest possible path. The route found by Bobbio *et al.* [5] had instead chosen straight lines with emphasis on binary and unary alloys. The new path also showcases how boundaries between systems are inconsequential when choosing a path through the continuous straight line from Cr-Fe-V to the Ti-V binary in the Cr-Ti-V system. While it is more efficient, it does lack certain considerations brought on by outside knowledge. One such example is that Fe-V alloys have considerable risk of σ phase formation as shown by the large infeasible region in Figure 5. Bobbio *et al.* [62] had also previously shown experimentally V to stainless steel FGMs cracked due to σ phase, which can be seen in the top-left part of Figure 5; thus, the avoidance of Fe-V may have played a role in choosing which systems to navigate by experts, while an automated search navigated around the problem in unbiased fashion and finding the shortest path while still ensuring avoidance of the σ phase.

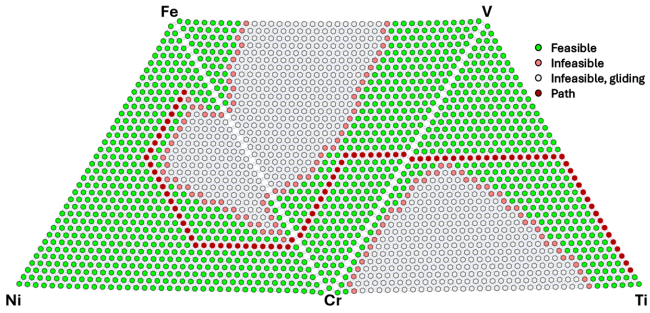

Figure 5: Subset of compositional graph containing only the 3 ternary systems traversed by the shortest feasible path with the identified path (crimson), feasible compositions (green), infeasible compositions (pink), and not-calculated interiors of the infeasible regions (gray).

4 Conclusions

Computational design of compositionally complex materials is a challenging task, especially when the design space has to account for manufacturing constraints while simultaneously handling calculations of constraints and objectives. `AMMap` is a novel open-source tool which enables users to define material space exploration and path planning problems in consistent, readable fashion, while building on top of existing literature tools treated as largely independent modules. Primary advantages of `AMMap` include:

- Automated generation of simplex (compositional) graph representations of the design space with `nimplex` [39] to allow for representation of elaborate design problem spaces in homogeneous fashion.
- Stitching of graphs utilizing different thermodynamic databases (TDBs) into singular traversable graph, allowing for fully automated path planning across composition regions which overlap but were not modeled together, which is a major obstacle in traditional joining of dissimilar materials.
- Infeasibility Gliding technique prevents exploration of internal infeasible regions to avoid unnecessary calculations (not contributing to pathfinding), drastically reducing total computational cost.

- Generation of modular callables for thermodynamic (equilibrium and Scheil-Gulliver) and other calculations to further inform material design or selection.

- Path planning deployment of established graph algorithms over the created design space, using a backend of choice.

To demonstrate the above advantages and automated space exploration with AMMap, the continuous path design has been conducted to connect a stainless steel and a titanium alloy alloy through 10 ternary systems, following on past studies [5]. The exploration has not only required just half of the computational cost, relative to traditional enumeration approach, but also identified a more optimal (shorter) path than chosen by previous works, by considering all 30 possible connections between underlying ternaries to find a non-obvious path requiring turning back.

5 Code Availability

AMMap code (beta version), examples, and other materials have been made public and are available in a GitHub repository at github.com/PhasesResearchLab/AMMap. Future releases will be published through the same repository, integrating additional functionalities. Instructions for installation and running of AMMap as well as how to add new properties as functions are included there.

Contributions CRediT

A. M. Richter: Conceptualization, Data Curation, Investigation, Methodology, Software, Validation, Writing - Original Draft, **A. M. Krajewski:** Conceptualization, Methodology, Software, Validation, Visualization, Writing - Original Draft, **Z. Yang:** Investigation, Methodology, Writing – Original Draft, **A. M. Beese:** Funding acquisition, Resources, Supervision, Writing - Review & Editing, **Z.-K. Liu:** Funding acquisition, Resources, Supervision, Writing - Review & Editing

Acknowledgments

This work has been funded through U.S. Office of Naval Research (ONR) awards **N00014-23-2721** and **N00014-21-1-2608**. Computational simulations were performed through allocation **DMR1400063** from the Advanced Cyberinfrastructure Coordination Ecosystem: Services & Support (ACCESS) program, which is supported by U.S. National Science Foundation grants **2138259**, **2138286**, **2138307**, **2137603**, and **2138296**.

Conflicts of interest

All authors declared there are no conflicts of interest

References

[1] M. Attaran, "The rise of 3-D printing: The advantages of additive manufacturing over traditional manufacturing," *Business Horizons*, vol. 60, no. 5, pp. 677–688, Sep. 2017. DOI: 10.1016/J.BUSHOR.2017.05.011.

[2] M. Rahman, K. S. Islam, T. M. Dip, *et al.*, "A review on nanomaterial-based additive manufacturing: dynamics in properties, prospects, and challenges," *Progress in Additive Manufacturing*, vol. 9, no. 4, pp. 1197–1224, Aug. 2024. DOI: 10.1007/S40964-023-00514-8/FIGURES/9. [Online]. Available: https://link.springer.com/article/10.1007/s40964-023-00514-8.

[3] D. C. Hofmann, S. Roberts, R. Otis, *et al.*, "Developing gradient metal alloys through radial deposition additive manufacturing," *Scientific Reports*, vol. 4, Jun. 2014. DOI: 10.1038/SREP05357.

[4] C. Zhang, F. Chen, Z. Huang, *et al.*, "Additive manufacturing of functionally graded materials: A review," *Materials Science and Engineering: A*, vol. 764, p. 138 209, 2019. DOI: 10.1016/j.msea.2019.138209.

[5] L. D. Bobbio, B. Bocklund, E. Simsek, *et al.*, "Design of an additively manufactured functionally graded material of 316 stainless steel and Ti-6Al-4V with Ni-20Cr, Cr, and V intermediate compositions," *Additive Manufacturing*, vol. 51, p. 102 649, Mar. 2022. DOI: 10.1016/J.ADDMA.2022.102649.

[6] D. C. Hofmann, J. Kolodziejska, S. Roberts, *et al.*, "Compositionally graded metals: A new frontier of additive manufacturing," DOI: 10.1557/jmr.2014.208.

[7] T. Kirk, E. Galvan, R. Malak, and R. Arroyave, "Computational Design of Gradient Paths in Additively Manufactured Functionally Graded Materials," *Journal of Mechanical Design*, vol. 140, no. 11, Nov. 2018. DOI: 10.1115/1.4040816. [Online]. Available: https://asmedigitalcollection.asme.org/mechanicaldesign/article/doi/10.1115/1.4040816/366178/Computational-Design-of-Gradient-Paths-in.

[8] T. Kirk, R. Malak, and R. Arroyave, "Computational design of compositionally graded alloys for property monotonicity," *Journal of Mechanical Design*, vol. 143, no. 3, Mar. 2021. DOI: 10.1115/1.4048627/1087579. [Online]. Available: https://dx.doi.org/10.1115/1.4048627.

[9] B. Bocklund, L. D. Bobbio, R. A. Otis, A. M. Beese, and Z.-K. Liu, "Experimental validation of Scheil–Gulliver simulations for gradient path planning in additively manufactured functionally graded materials," *Materialia*, vol. 11, p. 100 689, Jun. 2020. DOI: 10.1016/j.mtla.2020.100689. [Online]. Available: https://linkinghub.elsevier.com/retrieve/pii/S258915292030106X.

[10] B. Bocklund and Z.-K. Liu, "Computational Design of Additively Manufactured Functionally Graded Materials by Thermodynamic Modeling with Uncertainty Quantification," English, Ph.D. dissertation, The Pennsylvania State University, United States – Pennsylvania, 2021. [Online]. Available: https://etda.libraries.psu.edu/catalog/21192bjb54.

[11] A. R. Moustafa, A. Durga, G. Lindwall, and Z. C. Cordero, "Scheil ternary projection (STeP) diagrams for designing additively manufactured functionally graded metals," *Additive Manufacturing*, vol. 32, p. 101 008, Mar. 2020. DOI: 10.1016/j.addma.2019.101008. [Online]. Available: https://linkinghub.elsevier.com/retrieve/pii/S2214860419318305.

[12] Z. Yang, H. Sun, Z.-K. Liu, and A. M. Beese, "Design methodology for functionally graded materials: Framework for considering cracking," *Additive Manufacturing*, vol. 73, p. 103 672, 2023. DOI: 10.1016/j.addma.2023.103672. [Online]. Available: https://doi.org/10.1016/j.addma.2023.103672.

[13] H. Sun, B. Pan, Z. Yang, *et al.*, "MaterialsMap: A CALPHAD-based tool to design composition pathways through feasibility map for desired dissimilar materials, demonstrated with resistance spot welding joining of Ag-Al-Cu," *Materialia*, vol. 36, p. 102 153, Aug. 2024. DOI: 10.1016/j.mtla.2024.102153. [Online]. Available: https://linkinghub.elsevier.com/retrieve/pii/S2589152924001509.

[14] D. B. Miracle and O. N. Senkov, "A critical review of high entropy alloys and related concepts," *Acta Materialia*, vol. 122, pp. 448–511, Jan. 2017. DOI: 10.1016/J.ACTAMAT.2016.08.081.

[15] J. W. Yeh, S. K. Chen, S. J. Lin, *et al.*, "Nanostructured high-entropy alloys with multiple principal elements: Novel alloy design concepts and outcomes," *Advanced Engineering Materials*, vol. 6, no. 5, pp. 299–303, 2004. DOI: 10.1002/adem.200300567.

[16] B. Cantor, I. T. Chang, P. Knight, and A. J. Vincent, "Microstructural development in equiatomic multicomponent alloys," *Materials Science and Engineering A*, vol. 375-377, no. 1-2 SPEC. ISS. Pp. 213–218, Jul. 2004. DOI: 10.1016/j.msea.2003.10.257.

[17] O. N. Senkov, S. Gorsse, and D. B. Miracle, "High temperature strength of refractory complex concentrated alloys," *Acta Materialia*, vol. 175, pp. 394–405, Aug. 2019. DOI: 10.1016/j.actamat.2019.06.032.

[18] Z. Li, S. Zhao, R. O. Ritchie, and M. A. Meyers, "Mechanical properties of high-entropy alloys with emphasis on face-centered cubic alloys," *Progress in Materials Science*, vol. 102, pp. 296–345, May 2019. DOI: 10.1016/J.PMATSCI.2018.12.003.

[19] A. Debnath, A. M. Krajewski, H. Sun, *et al.*, "Generative deep learning as a tool for inverse design of high entropy refractory alloys," *Journal of Materials Informatics*, vol. 1, no. 1, p. 3, Sep. 2021. DOI: 10.20517/jmi.2021.05. [Online]. Available: https://www.oaepublish.com/articles/jmi.2021.05.

[20] C. Oses, C. Toher, and S. Curtarolo, "High-entropy ceramics," *Nature Reviews Materials*, vol. 5, no. 4, pp. 295–309, Feb. 2020. DOI: 10.1038/s41578-019-0170-8. [Online]. Available: https://www.nature.com/articles/s41578-019-0170-8.

[21] W. H. Wang, "High-Entropy Metallic Glasses," *JOM*, vol. 66, no. 10, pp. 2067–2077, Oct. 2014. DOI: 10.1007/s11837-014-1002-3. [Online]. Available: http://link.springer.com/10.1007/s11837-014-1002-3.

[22] Y. Huang, J.-W. Yeh, and A. C.-M. Yang, ""High-entropy polymers": A new route of polymer mixing with suppressed phase separation," *Materialia*, vol. 15, p. 100 978, Mar. 2021. DOI: 10.1016/j.mtla.2020.100978. [Online]. Available: https://linkinghub.elsevier.com/retrieve/pii/S258915292030394X.

[23] X. Hou, S. Chen, J. J. Koh, *et al.*, "Entropy-Driven Ultratough Blends from Brittle Polymers," *ACS Macro Letters*, vol. 10, no. 4, pp. 406–411, Apr. 2021. DOI: 10.1021/acsmacrolett.0c00844. [Online]. Available: https://pubs.acs.org/doi/10.1021/acsmacrolett.0c00844.

[24] T. Hirai, K. Yagi, K. Nakai, K. Okamoto, D. Murai, and H. Okamoto, "High-entropy polymer blends utilizing in situ exchange reaction," *Polymer*, vol. 240, p. 124 483, Feb. 2022. DOI: 10.1016/j.polymer.2021.124483. [Online]. Available: https://linkinghub.elsevier.com/retrieve/pii/S003238612101106X.

[25] O. Senkov, G. Wilks, D. Miracle, C. Chuang, and P. Liaw, "Refractory high-entropy alloys," *Intermetallics*, vol. 18, no. 9, pp. 1758–1765, Sep. 2010. DOI: 10.1016/j.intermet.2010.05.014. [Online]. Available: https://linkinghub.elsevier.com/retrieve/pii/S0966979510002475.

[26] K. Zhang, H. Wen, B. Zhao, X. Dong, and L. Zhang, "Precipitation behavior and its impact on mechanical properties in an aged carbon-containing Al0.3Cu0.5CrFeNi2 high-entropy alloy," *Materials Characterization*, vol. 155, p. 109 792, Sep. 2019. DOI: 10.1016/j.matchar.2019.109792. [Online]. Available: https://linkinghub.elsevier.com/retrieve/pii/S1044580319312410.

[27] Y. Long, X. Liang, K. Su, H. Peng, and X. Li, "A fine-grained NbMoTaWVCr refractory high-entropy alloy with ultra-high strength: Microstructural evolution and mechanical properties," *Journal of Alloys and Compounds*, vol. 780, pp. 607–617, Apr. 2019. DOI: 10.1016/J.JALLCOM.2018.11.318.

[28] O. Senkov, D. Isheim, D. Seidman, and A. Pilchak, "Development of a Refractory High Entropy Superalloy," *Entropy*, vol. 18, no. 3, p. 102, Mar. 2016. DOI: 10.3390/e18030102. [Online]. Available: http://www.mdpi.com/1099-4300/18/3/102.

[29] B. Kang, T. Kong, H. J. Ryu, and S. H. Hong, "Superior mechanical properties and strengthening mechanisms of lightweight AlxCrNbVMo refractory high-entropy alloys (x = 0, 0.5, 1.0) fabricated by the powder metallurgy process," *Journal of Materials Science & Technology*, vol. 69, pp. 32–41, Apr. 2021. DOI: 10.1016/j.jmst.2020.07.012. [Online]. Available: https://linkinghub.elsevier.com/retrieve/pii/S1005030220307179.

[30] G. Ouyang, P. Singh, R. Su, *et al.*, "Design of refractory multi-principal-element alloys for high-temperature applications," *npj Computational Materials*, vol. 9, no. 1, p. 141, Aug. 2023. DOI: 10.1038/s41524-023-01095-4. [Online]. Available: https://www.nature.com/articles/s41524-023-01095-4.

[31] Y. S. Lee and R. J. Cava, "Superconductivity in high and medium entropy alloys based on MoReRu," *Physica C: Superconductivity and its Applications*, vol. 566, Nov. 2019. DOI: 10.1016/j.physc.2019.1353520.

[32] X. Xu, W. Yang, H. Song, *et al.*, "Structural sequence and superconductivity in high-entropy Mo-W-Re-Ru-Pd alloys," *Scripta Materialia*, vol. 243, p. 115 986, Apr. 2024. DOI: 10.1016/j.scriptamat.2024.115986. [Online]. Available: https://linkinghub.elsevier.com/retrieve/pii/S1359646224000216.

[33] D. Strong and R. J. Cava, "Superconductivity in the face-centered cubic W-M-Rh-Ir-Pt M = {Mo, Nb, Ta, Re} high-entropy alloy," *Journal of Materials Science*, vol. 59, no. 23, pp. 10 347–10 356, Jun. 2024. DOI: 10.1007/s10853-024-09780-5. [Online]. Available: https://link.springer.com/10.1007/s10853-024-09780-5.

[34] C. Deng, T. Wang, P. Wu, W. Zhu, and S. Dai, *High entropy materials for catalysis: A critical review of fundamental concepts and applications*, Feb. 2024. DOI: 10.1016/j.nanoen.2023.109153.

[35] C. X. Han, J. Q. Zhi, Z. Zeng, *et al.*, "Synthesis and characterization of nano-polycrystal diamonds on refractory high entropy alloys by chemical vapour deposition," *Applied Surface Science*, vol. 623, Jun. 2023. DOI: 10.1016/j.apsusc.2023.157108.

[36] X. Li, C.-H. Shek, P. K. Liaw, and G. Shan, "Machine learning studies for magnetic compositionally complex alloys: A critical review," *Progress in Materials Science*, vol. 146, p. 101 332, Dec. 2024. DOI: 10.1016/j.pmatsci.2024.101332. [Online]. Available: https://linkinghub.elsevier.com/retrieve/pii/S0079642524001014.

[37] T. Zuo, M. C. Gao, L. Ouyang, *et al.*, "Tailoring magnetic behavior of CoFeMnNiX (X = Al, Cr, Ga, and Sn) high entropy alloys by metal doping," *Acta Materialia*, vol. 130, pp. 10–18, May 2017. DOI: 10.1016/j.actamat.2017.03.013.

[38] X. Feng, R. Zheng, Z. Wu, *et al.*, "Study on a new high-entropy alloy Nd20Pr20La20Fe20Co10Al10 with hard magnetic properties," *Journal of Alloys and Compounds*, vol. 882, Nov. 2021. DOI: 10.1016/j.jallcom.2021.160640.

[39] A. M. Krajewski, A. M. Beese, W. F. Reinhart, and Z.-K. Liu, "Efficient generation of grids and traversal graphs in compositional spaces towards exploration and path planning," *npj Unconventional Computing*, vol. 1, no. 1, p. 12, Nov. 2024. DOI: 10.1038/s44335-024-00012-2. [Online]. Available: https://www.nature.com/articles/s44335-024-00012-2.

[40] A. Rumpf, *Nim Programming Language v2.0.0*, 2023. [Online]. Available: https://nim-lang.org/.

[41] C. R. Harris, K. J. Millman, S. J. van der Walt, *et al.*, "Array programming with NumPy," *Nature*, vol. 585, no. 7825, pp. 357–362, Sep. 2020. DOI: 10.1038/s41586-020-2649-2. [Online]. Available: https://www.nature.com/articles/s41586-020-2649-2.

[42] P. Hart, N. Nilsson, and B. Raphael, "A Formal Basis for the Heuristic Determination of Minimum Cost Paths," *IEEE Transactions on Systems Science and Cybernetics*, vol. 4, no. 2, pp. 100–107, 1968. DOI: 10.1109/TSSC.1968.300136. [Online]. Available: http://ieeexplore.ieee.org/document/4082128/.

[43] R. Dechter and J. Pearl, "Generalized best-first search strategies and the optimality of A*," *Journal of the ACM*, vol. 32, no. 3, pp. 505–536, Jul. 1985. DOI: 10.1145/3828.3830. [Online]. Available: https://dl.acm.org/doi/10.1145/3828.3830.

[44] M Hillert, *Phase equilibria, phase diagrams and phase transformations: their thermodynamic basis*. 2007. [Online]. Available: https://books.google.com/books?hl=en&lr=&id=juk4cxteC1AC&oi=fnd&pg=PA3&ots=CxXkfkIsSI&sig=_ABXTD5Mmdw_wq1wErGJKR5ciCg.

[45] Z. Liu and Y Wang, *Computational thermodynamics of materials*. 2016. [Online]. Available: https://books.google.com/books?hl=en&lr=&id=Zm1eDAAAQBAJ&oi=fnd&pg=PA52&ots=WKyJEzSD8d&sig=t4MjW7-3hNsGkMOFkocILJybnd8.

[46] Z. K. Liu, "First-principles calculations and CALPHAD modeling of thermodynamics," *Journal of Phase Equilibria and Diffusion*, vol. 30, no. 5, pp. 517–534, Oct. 2009. DOI: 10.1007/S11669-009-9570-6.

[47] Z. K. Liu, "Computational thermodynamics and its applications," *Acta Materialia*, vol. 200, pp. 745–792, Nov. 2020. DOI: 10.1016/j.actamat.2020.08.008.

[48] Z.-K. Liu, "Thermodynamics and its prediction and CALPHAD modeling: Review, state of the art, and perspectives," *Calphad*, vol. 82, p. 102 580, Sep. 2023. DOI: 10.1016/j.calphad.2023.102580. [Online]. Available: https://linkinghub.elsevier.com/retrieve/pii/S0364591623000524.

[49] E. Scheil, "Bemerkungen zur Schichtkristallbildung," *International Journal of Materials Research*, vol. 34, no. 3, pp. 70–72, Mar. 1942. DOI: 10.1515/IJMR-1942-340303.

[50] G. G. J. I. Met and u. 1913, "The quantitative effect of rapid cooling upon the constitution of binary alloys," *books.google.comGH GulliverJ. Inst. Met, 1913•books.google.com*, [Online]. Available: https://books.google.com/books?hl=en&lr=&id=T7twT3MGPSkC&oi=fnd&pg=PA252&ots=t7fDxKUR43&sig=Q7lv1M9-XT_6U3rzNP9O6EC_DRY.

[51] R. Otis and Z.-K. Liu, "pycalphad: CALPHAD-based Computational Thermodynamics in Python," *Journal of Open Research Software*, vol. 5, pp. 1–11, 2017. DOI: 10.5334/jors.140.

[52] Z. Yang, H. Sun, S. L. Shang, Z. K. Liu, and A. M. Beese, "Effect of heat treatment on functionally graded 304L stainless steel to Inconel 625 fabricated by directed energy deposition," *Materialia*, vol. 34, p. 102 067, May 2024. DOI: 10.1016/J.MTLA.2024.102067.

[53] B. E. Carroll, R. A. Otis, J. P. Borgonia, *et al.*, "Functionally graded material of 304L stainless steel and inconel 625 fabricated by directed energy deposition: Characterization and thermodynamic modeling," *Acta Materialia*, vol. 108, pp. 46–54, Apr. 2016. DOI: 10.1016/j.actamat.2016.02.019.

[54] L. D. Bobbio, B. Bocklund, Z. K. Liu, and A. M. Beese, "Tensile behavior of stainless steel 304L to Ni-20Cr functionally graded material: Experimental characterization and computational simulations," *Materialia*, vol. 18, Aug. 2021. DOI: 10.1016/J.MTLA.2021.101151.

[55] N. Chen, H. A. Khan, Z. Wan, *et al.*, "Microstructural characteristics and crack formation in additively manufactured bimetal material of 316L stainless steel and Inconel 625," *Additive Manufacturing*, vol. 32, Mar. 2020. DOI: 10.1016/j.addma.2020.101037.

[56] T. Li, Z. Wang, S. Hu, Z. Yang, and Y. Wang, "Hot cracking during the fabrication of Inconel 625/stainless steel 308 L functionally graded material by dual-wire arc additive manufacturing," *Journal of Manufacturing Processes*, vol. 82, pp. 461–473, Oct. 2022. DOI: 10.1016/j.jmapro.2022.08.018.

[57] H. Yu, J. Liang, Z. Bi, J. Li, and W. Xu, "Computational Design of Novel Ni Superalloys with Low Crack Susceptibility for Additive Manufacturing," *Metallurgical and Materials Transactions A: Physical Metallurgy and Materials Science*, vol. 53, no. 6, pp. 1945–1954, Jun. 2022. DOI: 10.1007/S11661-022-06653-X/TABLES/3. [Online]. Available: https://link.springer.com/article/10.1007/s11661-022-06653-x.

[58] M. Easton, M. Gibson, S Zhu, T. A. M. Materials, and u. 2014, "An A Priori Hot-Tearing Indicator Applied to Die-Cast Magnesium-Rare Earth Alloys," *SpringerMA Easton, MA Gibson, S Zhu, TB AbbottMetallurgical and Materials Transactions A, 2014•Springer*, vol. 45, no. 8, pp. 3586–3595, 2014. DOI: 10.1007/s11661-014-2272-7. [Online]. Available: https://link.springer.com/article/10.1007/s11661-014-2272-7.

[59] C. Tandoc, Y.-J. Hu, L. Qi, and P. K. Liaw, "Mining of lattice distortion, strength, and intrinsic ductility of refractory high entropy alloys," *npj Computational Materials*, vol. 9, no. 1, p. 53, Apr. 2023. DOI: 10.1038/s41524-023-00993-x. [Online]. Available: https://www.nature.com/articles/s41524-023-00993-x.

[60] Y.-J. Hu, A. Sundar, S. Ogata, and L. Qi, "Screening of generalized stacking fault energies, surface energies and intrinsic ductile potency of refractory multicomponent alloys," *Acta Materialia*, vol. 210, p. 116 800, May 2021. DOI: 10.1016/j.actamat.2021.116800. [Online]. Available: https://linkinghub.elsevier.com/retrieve/pii/S1359645421001804.

[61] A. Debnath, L. Raman, W. Li, *et al.*, "Comparing forward and inverse design paradigms: A case study on refractory high-entropy alloys," *Journal of Materials Research*, vol. 38, no. 17, pp. 4107–4117, Sep. 2023. DOI: 10.1557/s43578-023-01122-6. [Online]. Available: https://link.springer.com/10.1557/s43578-023-01122-6.

[62] L. D. Bobbio, B. Bocklund, R. Otis, *et al.*, "Characterization of a functionally graded material of Ti-6Al-4V to 304L stainless steel with an intermediate V section," *Journal of Alloys and Compounds*, vol. 742, pp. 1031–1036, Apr. 2018. DOI: 10.1016/J.JALLCOM.2018.01.156.